Solar Eclipse and Cosmic Ray Flux

Cite as: Phys. Teach. **60**, 100 (2022); https://doi.org/10.1119/10.0009417
Published Online: 31 January 2022

Tamar A. Dallal, Jacob M. Miller, Michelle Matten, et al.

Solar Eclipse and Cosmic Ray Flux

Tamar A. Dallal, Jacob M. Miller, Michelle Matten, Ezra Schur, and Allen J. Sears, Ida Crown Jewish Academy, Skokie, IL
Clarissa Carr, Jacob Rosenberg, Nathan A. Unterman (emeritus), and Anthony Valsamis, Glenbrook North High School, Northbrook, IL
Mark Adams, QuarkNet, Batavia, IL

During the August 21, 2017, solar eclipse, high school students measured secondary cosmic ray flux using QuarkNet[1] detectors. These students conducted experiments examining cosmic ray flux, shower, speed of muons, and muon lifetime using QuarkNet cosmic ray muon detectors (CRMDs).[2] These detectors measure muon flux of momenta greater than ~2 GeV, a threshold imposed by deflection due to Earth's magnetic field. This study utilized CRMDs, which are readily available for students, to investigate any deviation in secondary cosmic ray flux resulting from a solar eclipse. Other groups have conducted experiments regarding cosmic rays during eclipses[3-6]: Kandemir et al. reported on low-energy muons (under 1 GeV) during the eclipse of August 11, 1999; Nayak et al. and Bhaskar et al. studied air showers for gamma ray point sources; and Nishina et al. studied muon flux during a 1936 eclipse. Cosmic rays are charged particles created in exploding stars and active galaxies and travel through interplanetary space at relativistic velocities. The flux is largely unchanged between day and night, when Earth blocks the Sun, and the presence of the Sun and Moon has little effect.[7-9] A total eclipse provides a dramatic opportunity to search for that fraction of cosmic rays created by the Sun that are intercepted by the Moon. We hypothesized that muon flux will change during a total solar eclipse; however, we designed the experiment to search for signals at various angular scales near the direction of the Sun and to set upper limits on production from the Sun if no signal was observed.

Feasibility and design

The goal of the experiment was to measure muon flux baselines with multiple telescopes sensitive to different regions of the sky during times that the Moon, Sun, or neither (empty sky) were in the detectors' angle of acceptance. Differences observed during the eclipse would be evidence of a source of cosmic rays from the Sun itself.

This study utilized CRMDs built with four scintillator counters; by separating the counters and overlapping them, a narrow angle of acceptance was isolated so muon events were measured in the proximity of the eclipsed region of the sky. Muon coincident events are recorded when at least two counters of the CRMD are struck within a small time interval. A feasibility study was conducted to evaluate if four scintillator counters could observe muon coincidences within a small portion of the sky while still maintaining statistically significant measurements during the eclipse.

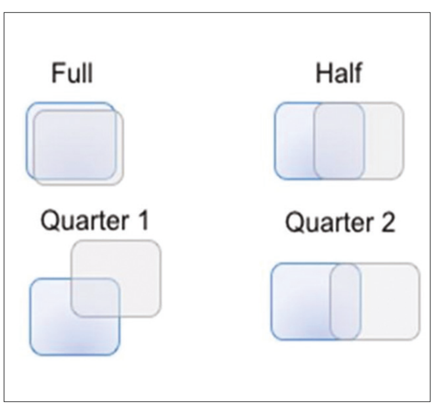

Fig. 1. Test configurations of counters in pre-study. The Quarter 1 design was selected. The long diagonal axis was oriented east-west in the fixed and tracking telescopes and oriented north-south in a second tracking telescope.

Three main overlap schemes were considered: counters that overlapped full-full, with counters completely overlapped; half-half, with half of each counter overlapping half of the other; and quarter-quarter, such that a quarter of one counter overlapped with a quarter of another (Fig. 1). The overlapping schemes yielded a linear relationship (Fig. 2) between muon rate and area of overlap.

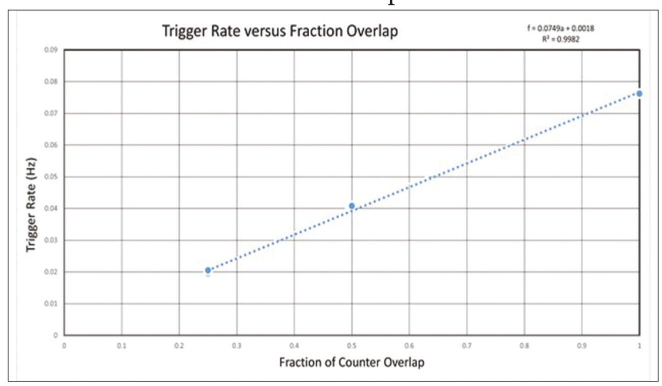

Fig. 2. Measurement of trigger rate during detector testing to determine the optimal area of detector overlap. The statistical errors are less than 0.3% per point.

To narrow the angle of acceptance of the detector, pairs of scintillators were separated by various distances. To test the most effective distance to isolate the desired region in the sky while maintaining statistically significant counts, trials were run with detectors separated at different distances. Greater separations between pairs of overlapped scintillators resulted in smaller angles of acceptance and lower counts. For a pair of counters to function like a telescope, defining a direction, one muon must traverse both counters. The background caused by two or more muons in a cosmic ray shower from a different direction was measured to be less than 3%.

Angular acceptance for a pair of 25 cm x 30 cm counters was calculated by a simple Monte Carlo simulation of muon trajectories that intercept both counters. We define an effective angular acceptance, wherein 90% of trajectories hitting both counters are captured (to avoid being too sensitive to the small number of events at large angles from corners), and find that to be consistent with 70% of the maximum one-dimensional angle from an edge of one counter to the opposite edge of the second counter.

The final study involved four CRMDs: two detectors that tracked the Sun throughout the eclipse (tracking telescopes), a static detector aimed at the center of totality throughout the experiment (fixed telescope), and a vertically stacked detector aimed at the zenith (control). To enlarge the angular acceptance in a certain direction, the two tracking telescopes were

 DOI: 10.1119/10.0009417

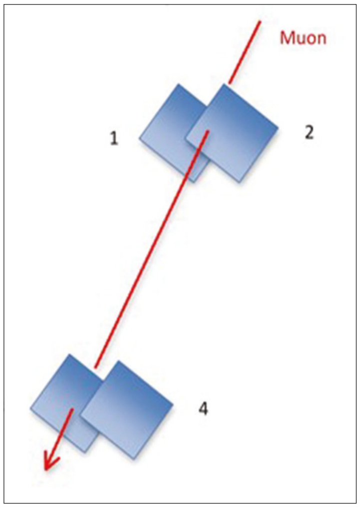

Fig. 3. The finalized detector design consisted of two pairs of two counters separated a set distance. Both pairs of overlapped counters were overlapped with a quarter-quarter design.

Fig. 4. Tracking telescope; note the placement of the counters in the overlapping quarter-quarter design.

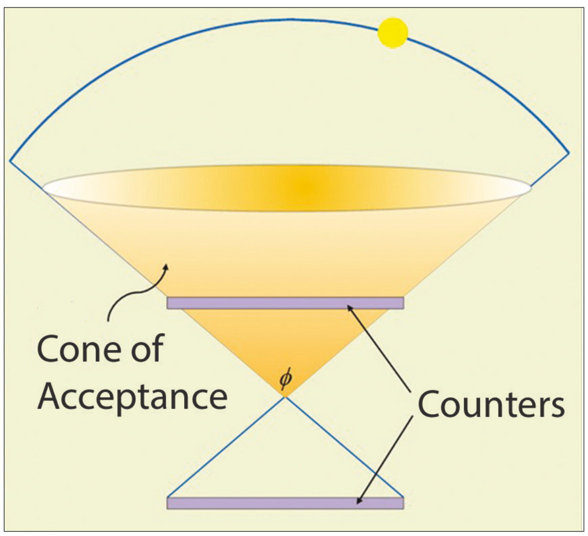

Fig. 5. Diagram of the telescope that includes two separated counters, creating an angle of acceptance of Φ.

constructed with the offset counter placement biased east-west (EW) in one telescope and north-south (NS) in the other, thereby sensitive to differences in flux due to geomagnetic deflection. The fixed telescope had a wide angle of acceptance to measure first through fourth contact. To collect additional control samples, detectors were also operated at locations outside the path of the eclipse (results not included in this article).

The finalized design involved a quarter-quarter overlap scheme with two pairs of two counters separated by two meters for a fixed telescope and three meters for a tracking telescope (Figs. 3 and 4). This allowed for measuring flux with different angles of acceptance (Fig. 5) and isolating eclipse effects, all while maintaining sufficient counts for statistical significance. When on-axis pairs of scintillators (e.g., *13* and *24*)[10] were analyzed, the angle of acceptance was 11° for the fixed detector; off-axis pairs (*14* and *23*) enlarged the acceptance along the overlap direction to 22.3°. Angular acceptances were 7.3° and 14.9° for the tracking detectors, 3.1° for four-fold coincidences (*1234*). The control detector had an acceptance of 89° encompassing the zenith.

To establish baseline rates, the fixed telescope recorded events during transits of the Sun and Moon as well as during empty sky periods in the days leading up to the eclipse. The tracking telescopes recorded events during the same periods but followed the path of the Sun.

Normalization and data quality monitoring

Muon rates are inversely proportional to atmospheric pressure.[11] Instead of correcting for pressure, muon fluxes from different time periods were normalized using the ratio of rates in the control detector in those same periods.

Data were binned in 10-minute intervals for data analysis. Although the period of totality was just over 2.5 minutes at Jefferson College in Hillsboro, MO,[12] the time from first to last contact of the Moon and Sun was 175 minutes. To monitor the stability of individual counters of the fixed detector over time, rates from pairs of counters pointing toward the Sun were compared with rates from pairs with larger angles of acceptance. The data from the tracking detectors were corrected by $\sin^2\theta$,[13] a function of the Sun's angle of elevation θ. During separate empty sky calibration runs, muon rates were measured vs. θ and found to be consistent with $\sin^2\theta$ over the angles encountered during the eclipse.

Findings

The three stages of analysis were to identify stable running periods by comparing relative internal rates, searching for structure during transits or the eclipse, and calculating an upper limit on muons from the Sun. Muon rates for counter pairs pointing near the Sun in the fixed detector are shown for the day of the eclipse (Fig. 6). Cables supplying voltage to photomultiplier tubes on the counters in the fixed detector proved unstable in the extreme heat during earlier data taking and were replaced. Operation of channel 2 remained unstable, so it was excluded from final eclipse analysis to keep systematic errors small. On the day of the eclipse, the high voltage (HV)

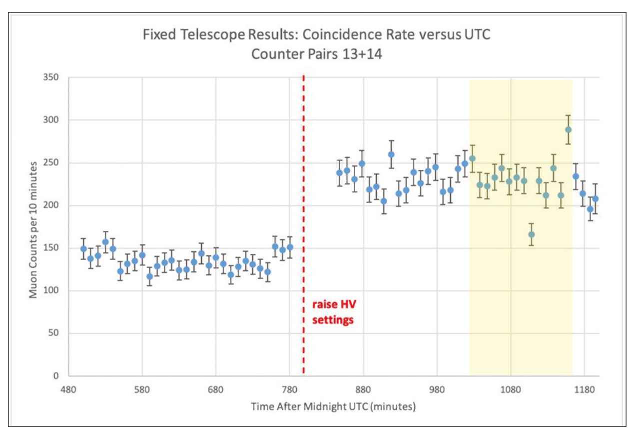

Fig. 6. Fixed telescope results: number of muons (*13+14*) every 10 minutes since midnight UTC. HV to counters was increased to raise efficiency around 790 minutes (red dashed line). The eclipse period is shaded in yellow.

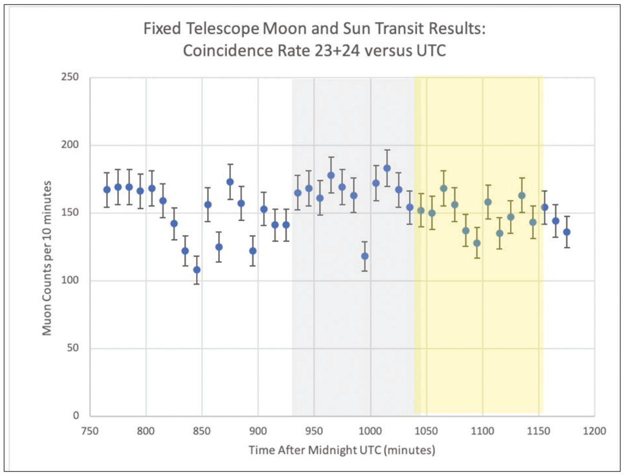

Fig. 7. Fixed telescope results for lunar (gray) and solar (yellow) transits, muons (*23+24*) every 10 minutes since midnight UTC.

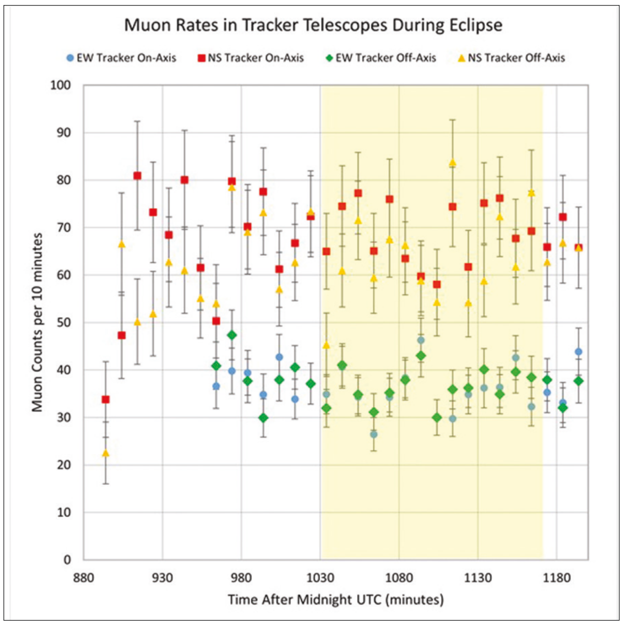

Fig. 8. Tracking telescope results of muon events per 10 minutes since midnight UTC. Presented are rates corrected for elevation: on-axis (*13+24*) for the EW (NS) tracker in blue circles (red squares); off-axis (*14*+23) for the EW (NS) tracker in green diamonds (yellow triangles). The yellow highlighted area marks the time interval of the eclipse.

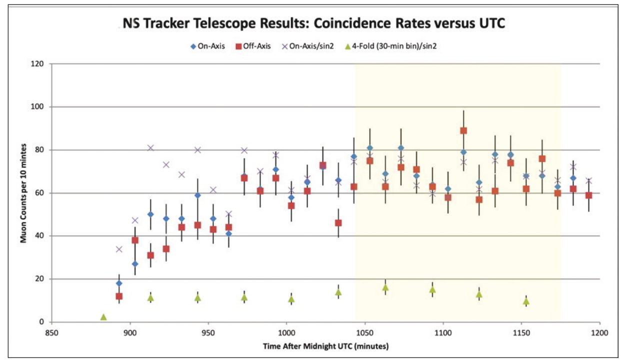

Fig. 9. NS Tracking telescope results near the eclipse of muon events per 10 minutes since midnight UTC with double counting due to overlapping events *1234* removed. Presented are raw muon rates for the on-axis rates (*13+24-1234*) in blue circles and off-axis rates (*13+24-1234*) in red squares. The on-axis rates corrected for elevation are shown purple x markers. The narrow angular acceptance four-fold triggers (*1234*) corrected for elevation are displayed in green triangles. The yellow highlighted area marks the time interval of the eclipse.

to all counters was increased to make counters more efficient. Therefore, rates of empty sky were restricted to after the HV change when compared to the rates during the eclipse. All data, normalized or not, obtained during the eclipse from the fixed telescope exhibit constant behavior. Pre-eclipse studies of solar and lunar transits indicate that the celestial bodies entering the detector's cone of acceptance yielded no significant change in the number of events (Fig. 7), demonstrating shadowing effects to be negligible. Data taken during the eclipse revealed no measurable divergence from baselines.

Counts from the telescopes that tracked the Sun throughout the eclipse are compared to the EW and NS telescopes in the direction aligned with the Sun (Fig. 8) using on-axis counters *13* and *24* and off-axis counters *14* and *23*. As the Moon entered and exited the detector's cone of acceptance, rates for all four conditions are similar. Results of additional analysis are shown for the NS tracking detector (Fig. 9). Double counting is removed by subtracting the four-fold coincidences. The on-axis rate corrected by $\sin^2\theta$ illustrates that the eclipse resulted in no significant change in the number of events within the limits of our statistics. The data from the smaller rate of the four-fold coincidence are shown in 30-minute bins and also exhibit no structure during the eclipse.

Statistical analysis

Since no structure in muon rates at any angular scale was observed within statistical errors, we chose to compare the average muon rates during the eclipse to rates from the empty sky during the period of most stable data collection. The standard statistical error of a normal distribution for measuring N counts is $\sqrt{N}$. The statistical error of each muon rate is given by the mean value of the rate times the percent statistical error ($1/\sqrt{N}$). Systematic errors are small compared to the statistical errors. For this analysis, events from detector pairs *13* and *14* within the fixed telescope were used. Fixed telescope data are presented in Table I, and tracking data are in Table II. The ratio of muon flux for the fixed telescope during the eclipse to the flux during the empty sky period is 0.981 ± 0.026. This is consistent with no signal from the Sun. The same ratio for the NS tracking telescope is 0.997 ± 0.037. A similar comparison of rates in the control detector, utilizing a full day of empty sky data corrected for atmospheric pressure (using control detector calibration Δrate/Δpressure = –0.0062/mb), yields 1.002 ± 0.005. No signal is observed above the statistical error in any telescope.

To set the 95% confidence level upper limit on a signal from the Sun, using the fixed detector, we calculate the fraction of events that fall over 2σ away from the mean and determine that less than 5.2% of the muons in the direction from the Sun originate from the Sun. Since the fraction of muons detected by the fixed telescope near the position of the Sun is only 1.4% of the total muon rate we measure from the full sky,

Table I. Displayed are muon counts in the fixed detector for empty sky and eclipse periods used in the calculation of the ratio. Presented are the data period; average counts per 10 minutes for counter pairs *13*, *14*, and *34*; total number of events *N* = *13*+*14*; the percent error (1/√*N*); and normalization of periods from the control detector.

Fixed Detector	Period (min)	Counts *13* 10-min average	Counts *14* 10-min average	Counts *34* 10-min average	Total Events (*13*+*14*)	Percent Error	Normalized with control detector
Eclipse	90	110.6	114.3	2318	2024	2.2	1.000
Empty	200	113.9	116.2	2329	5062	1.4	0.996

Table II. Displayed are muon counts in the NS tracking detector for empty sky and eclipse periods used in the calculation of the ratio. Presented are the sample period, average counts per 10 minutes for counter pairs on-axis and off-axis, the percent error (1/√*N*), and normalization from the control detector defining the rate during the eclipse as 1. The final empty period muon rates corrected for normalization and elevation effects are also shown.

NS Tracking Detector	Period (min)	On-axis 10-min average	Off-axis 10-min average	On-axis Corrected: Normalize + Elevation	Off-axis Corrected: Normalize + Elevation	Percent Error	Normalized with control detector
Eclipse	100	72.4	67.2	72.4	67.2	3.7	1.000
Empty	4200	74.8	70.1	72.6	68.0	0.6	0.990

under the assumption that any effect would be located near the Sun, this implies that less than 7×10^{-4} of all muons can be attributed to the Sun. This is a factor greater than 10 improvement over the previously published result[6] from 1936.

Conclusion

Results from this study show no signal near the direction of the Sun beyond empty sky rates in cosmic ray muon events during the eclipse at angular scales from 7.4° to 32°. The Sun and Moon are neither sources nor blockers of cosmic rays muons with energies 2 GeV and higher, within our statistical errors. Using the fixed detector, a 95% confidence level upper limit of 5.2% is set on the source of muons from the Sun.

This QuarkNet project includes other participating schools; data from over 25 other schools' locations can be mined as a source for classroom activities for college students and advanced high school students. Our study could be further improved by considering additional detectors and locations of detectors as a function of distance from the region of totality. After our exploration, we became aware of simulations for an investigation conducted in Tibet[14] suggesting that an eclipse signal might be found elsewhere in the sky, not necessarily in the eclipse region. Since the magnitude of this offset is inconsistent with calculations from the Main Injector Neutrino Oscillation Search (MINOS)[15] articles we used in designing our detector's acceptance, we decided to treat the difference as a systematic error and quote our limit for muons of greater than 5 GeV energy (rather than the normal 2 GeV threshold). This consideration would contribute to baseline studies and alternate detector aiming in future eclipse experimental designs. An eclipse's effect on muon events might also occur before or after the eclipse, outside the time frame measured in this study. Since our measurement was constrained by the number of muons detected, a larger collecting surface area would improve the limit. We look forward to testing some of these possibilities in 2024!

Acknowledgments

Robert Brazzle and Jefferson College, Hillsboro, MO, for hosting our group; QuarkNet; National Science Foundation; U.S. Department of Energy; Administrations of the respective high schools; Eleanor Hamilton, Jill Serling, and Marie Self for their support of this opportunity.

References

1. Carol Polen, "Particle physics: An essential and engaging part of the high school physics program," *Phys. Teach.* **57**, 320–322 (May 2019).
2. *QuarkNet/Walta/CROP Cosmic Ray Detectors User's Manual* (2004), http://quarknet.fnal.gov/toolkits/ati/det-user.pdf .
3. G. Kandemir et al., "Variation of cosmic ray intensity during the solar eclipse August 11, 1999," *Last Total Solar Eclipse of the Millennium, APS Conference Series* **205**, 202–207 (ASP, Turkey, 2000), http://adsabs.harvard.edu/full/2000ASPC..205..202K.
4. Pranaba K. Nayak et al., "A study of the γ -ray flux during the total solar eclipse of 1 August 2008 at Novosibirsk, Russia," *Astropart. Phys.* **32** (6), 286–293 (2009).
5. Ankush Bhaskar et al., "A study of secondary cosmic ray flux variation during the annular eclipse of 15 January 2010 at Rameswaram, India," *Astropart. Phys.* **35** (5), 223–229 (2011).
6. Y. Nishina et al., "Measurements of cosmic rays during the solar eclipse of June 19, 1936," *Jpn. J. Astron. Geophys.* **14**, 265 (1936).
7. M. G. Aartsen et al. (IceCube Collaboration), "Observation of the cosmic-ray shadow of the Moon with IceCube," *Phys. Rev. D* **89**, 102004 (2014).
8. N. Giglietto (MACRO Collaboration), "Moon and Sun shadowing observed by the MACRO detector" (ICRC, South Africa,

1999), https://arxiv.org/abs/hep-ex/9905026.

9. In 2015, our QuarkNet group observed an effect with surface muons consistent with a 10% decrease in the low-energy muon flux in the direction of the Sun that spanned 30° east-to-west. This shadowing effect is too small to be statistically observed during the periods of transits.

10. Starting from the top of the telescope and moving down, the counters are numbered 1 through 4. The notation *14* denotes events within counters 1 and 4. Other combinations follow this convention.

11. J. Poirier and T. Catanach, "Atmospheric effects on muon flux at Project GRAND," *Proceedings of the 32nd International Cosmic Ray Conference* **11**, 348-351 (ICRC, China, 2011), DOI: 10.7529/ICRC2011/V11/0307.

12. 38:15.675097 N, 090:33.451804 W.

13. J. J. Beatty, J. Matthews, and S. P. Wakely, "Cosmic rays," Particle Data Group (2019), https://pdg.lbl.gov/2019/reviews/rpp2019-rev-cosmic-rays.pdf.

14. M. Storini, D. F. Smart, and M. A. Shea "Cosmic ray asymptotic directions for Yangbajing (Tibet) experiments," *Proceedings of the 27th International Cosmic Ray Conference* (ICRC, Germany, 2001), pp. 4106-4109.

15. P. Adamson et al., "Observation in the MINOS far detector of the shadowing of cosmic rays by the Sun and Moon," *Astropart. Phys.* **34**, 457–466 (2011).

Ida Crown Jewish Academy, Skokie, IL; tdallal2@illinois.edu